Inorganic Chemistry

Article

pubs.acs.org/IC

Metal–Ligand Cooperation in H_2 Activation with Iron Complexes Bearing Hemilabile Bis(diphenylphosphino)amine Ligands

Nicolas Frank,[†] Katharina Hanau,[†] and Robert Langer*[,†,‡]

[†]Department of Chemistry, Philipps-Universität Marburg, Hans-Meerwein-Str., 35043 Marburg, Germany

[‡]Lehn Institute of Functional Materials (LIFM), Sun Yat-Sen University (SYSU), Xingang Road West, Guangzhou 510275, P. R. China

Supporting Information

ABSTRACT: The octahedral transition-metal complex [(dppa)Fe(Ph_2P–N–PPh_2)$_2$] (**1**) [dppa = bis(diphenylphosphino)amine] with homofunctional bidentate ligands is described. The ligand exhibits hemilability due to its small bite angle and the steric repulsion of the coordinated donor groups. As the {Ph_2P–N–PPh_2}$^-$ ligand can act as an internal base, heterolytic cleavage of dihydrogen by complex **1** leads to the formation of the hydride complex [(dppa)(Ph_2P–N–PPh_2)Fe(H)(κ^1-Ph_2P–NH–PPh_2)$_2$] (**2**), representing an example of cooperative bond activation with a homofunctional hemilabile ligand. This study demonstrates that hemilability of homofunctionalized ligands can be affected by careful adjustment of geometric parameters.

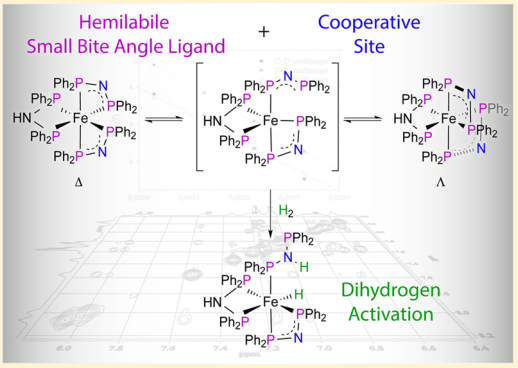

INTRODUCTION

Bond activation processes facilitated by cooperation of the central metal atom and a coordinated ligand in transition-metal complexes are key steps in biological and chemical catalysis, enabling the cleavage of substrate bonds without a formal change in the oxidation state.[1] This concept has led to new catalytic reactions[2] as well as to the development of non-noble-metal-based catalysts for known reactions in recent years.[3−6]

For many of these homogeneous catalysts, the reversible generation of a vacant coordination site by a hemilabile ligand and the presence of a cooperative site in the ligand that allows for the reversible acceptance of protons (or electrons) is essential for the observed catalytic activity. Such a hemilabile ligand can protect highly reactive intermediates by reversible bond formation between the labile donor group and the central metal atom, thus preventing undesired redox processes and immediate decomposition of the metal complex. Hybrid ligands featuring different donor functionalities often exhibit such hemilabile behavior when they are bound to a transition metal (Scheme 1).[7] In particular, for pincer-type ligands the hemilabile coordination of one "arm" often has a significant effect on the reactivity[8] and catalytic activity[9] of these complexes. In contrast, hemilability of homofunctional ligands in chelating transition-metal complexes and subsequent bond activation processes have not been reported to date, although substitution under arm opening by one carbon monoxide ligand has been shown for rhodium(I) complexes with tripodal phosphine ligands at high pressures.[10]

The growing interest in first-row transition-metal catalysts requires new strategies for the design of cooperative catalysts in order to circumvent undesired one-electron redox processes.

Scheme 1. Previously Reported and New Concepts for Ligand Hemilability

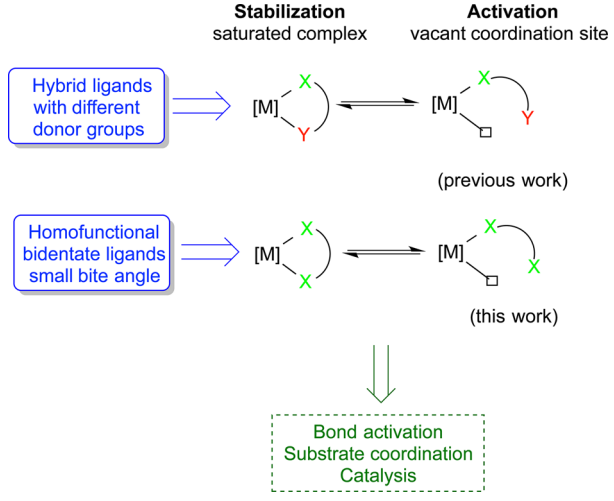

Especially iron complexes have attracted increased attention as potential substitutes for noble-metal catalysts because of the high abundance, low price, and low environmental impact of iron.[11] However, although an increasing number of iron catalysts have been reported, detailed mechanistic understanding that could allow for improvement and the development of new catalysts remains limited. While in many

Received: September 15, 2014
Published: October 7, 2014

   dx.doi.org/10.1021/ic5022164 | *Inorg. Chem.* 2014, 53, 11335−11343

hydrogenation reactions heterolytic cleavage of dihydrogen is rate-determining,[12] the unsaturated intermediate that allows for dihydrogen binding has often proved to be very unstable in the case of iron, thereby limiting catalytic applications.[5,6,13] Although heterolytic cleavage of dihydrogen across iron–nitrogen[14] and iron–boron bonds[15] as well as by pendant bases has been reported,[5,16] hemilability for bond activation with iron complexes is unprecedented.

Herein we describe a transition-metal complex with homofunctional bidentate ligands that exhibit hemilability due to the small ligand bite angle and the steric repulsion of the coordinated donor groups. The activation parameters of this process were determined for the unique octahedral iron(II) complex **1** with bis(diphenylphosphino)amine (dppa) and -amide (dppa*) ligands. Importantly, this complex readily reacts with dihydrogen to form of a hydride ligand and a protonated κ^1-coordinated dppa ligand, rendering a unique example of cooperative bond activation with a homofunctional hemilabile ligand.

RESULTS AND DISCUSSION

The reaction of $[Fe(N(SiMe_3)_2)_2(thf)]$ with 2 or 3 equiv of dppa in toluene leads to the formation of a new iron complex (Scheme 2) whose $^{31}P\{^1H\}$ NMR spectrum exhibits two

Scheme 2. Synthesis of Complex 1 (Only the Δ Isomer Is Shown)

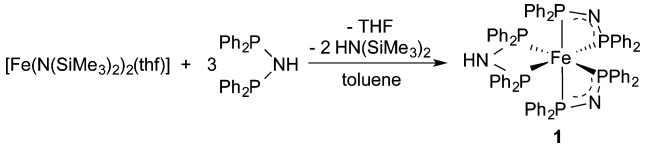

1

multiplet resonances at 4.5 and 64.7 ppm as well as one triplet of triplets resonance centered at 13.0 ppm. This observation indicates the formation of a diamagnetic octahedral iron(II) complex with three magnetically inequivalent kinds of phosphorus atoms. In contrast, the analogous reaction with bis(diisopropylphosphino)amine does not lead to any diamagnetic product, suggesting that this ligand is too bulky to coordinate 3 equivalents.

A structural analysis by single crystal X-ray diffraction confirmed the formation of a distorted octahedral complex in which the central iron atom is bound to three dppa or dppa* ligands (Figure 1). As a result of the small bite angle of these ligands, which was found to be between 65.56(4) and 69.23(4)° in **1**, the complex is twisted toward a trigonal-prismatic geometry with a twist angle of approximately 38.62°. At 2.316(1)–2.367(1) Å, the iron–phosphorus distances are rather long for octahedral iron(II) complexes, which might be caused by the steric overload of six PPh_2 groups. Similar Fe–P distances have been observed in the few reported examples of octahedral iron complexes with six tertiary phosphine groups coordinated.[17] As no counterions could be located, for charge balance two of the three dppa ligands are supposed to be deprotonated. In fact, the P–N distances to N1 [1.675(4)–1.678(4) Å] are slightly longer than the P–N distances to N2 and N3 [1.643(3)–1.656(4) Å], which is in agreement with the formula $[(dppa)Fe(Ph_2P–N–PPh_2)_2]$ (**1**). Furthermore, the P–Fe–P bite angle of the dppa ligand [∠P1–Fe1–P2 = 69.23(4) Å] is larger than the bite angles of the deprotonated ligands [∠P–Fe–P = 65.56(4)–65.71(4) Å]. Complex **1** is

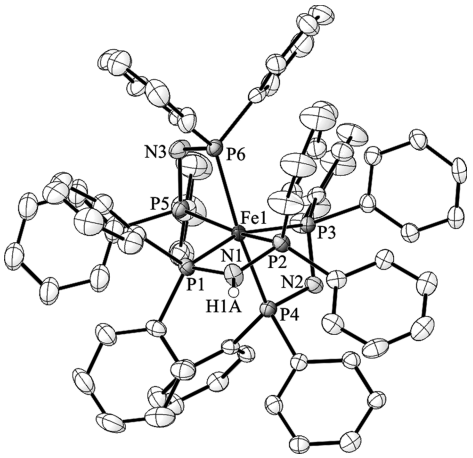

Figure 1. ORTEP diagram of $[(dppa)Fe(Ph_2P–N–PPh_2)_2]$ (**1**) with the thermal ellipsoids set at 50% probability (selected hydrogen atoms and solvent molecules have been omitted for clarity). Selected distances [Å] and angles [deg]: Fe1–P1 2.316(1), Fe1–P2 2.337(1), Fe1–P3 2.365(1), Fe1–P4 2.351(1), Fe1–P5 2.337(1), Fe1–P6 2.367(1), P1–N1 1.678(4), P2–N1 1.676(4), P3–N2 1.655(4), P4–N2 1.643(3), P5–N3 1.644(4), P6–N3 1.646(4); P1–Fe1–P2 69.23(4), P4–Fe1–P3 65.71(4), P5–Fe1–P6 65.56(4).

chiral and crystallizes with only one enantiomer in each crystal. Although three different batches were analyzed using single-crystal X-ray diffraction, we always identified the Δ isomer as the only enantiomer present.

In accordance with the molecular structure in the crystal lattice, we were able to identify six spin systems between 6.50 and 8.20 ppm in the ^1H NMR spectrum, corresponding to the 12 phenyl rings in **1**. In addition, the ^1H NMR spectrum of complex **1** in C_6D_6 revealed a broad resonance at 4.61 ppm that shows a nuclear Overhauser effect (NOE) cross-peak to two different *o*-phenyl protons in the ^1H *g*NOESY NMR spectrum (Figure 2, right). Interestingly, for several resonances in the aromatic region, cross-peaks with the same phase as the diagonal peak could be observed in the ^1H *g*NOESY NMR spectrum, suggesting chemical exchange between these atoms. A closer look at the well-separated resonances of the *o*-phenyl protons revealed that the signals of the protonated dppa ligand (E and F) show cross-peaks corresponding to chemical exchange (Figure 2, right) in addition to the observed NOE contacts to the NH proton. Furthermore, the remaining four *o*-phenyl resonances of the two deprotonated dppa ligands (A–D) display cross peaks due to chemical exchange as well (Figure 2, right). In part, some of the detected exchange processes would be in agreement with a racemization equilibrium between the Δ and Λ isomers in solution, while the NH proton seems to be well-located and does not show any exchange. This finding is underlined by the fact that in the presence of excess dppa no exchange could be observed between the uncoordinated dppa ligand and the coordinated dppa in complex **3**.

Such an intramolecular exchange can proceed via different isomerization pathways with different intermediates (Figure 2, left). For octahedral transition-metal complexes, the commonly proposed mechanisms are nondissociative processes that proceed through a C_{2v}-symmetric transition state (**A**) in the case of the Ray–Dutt twist or a D_{3h}-symmetric transition state (**C**) in case of the so-called Bailar twist. In addition, dissociative isomerization pathways have been identified for some metal

dx.doi.org/10.1021/ic5022164 | Inorg. Chem. 2014, 53, 11335–11343

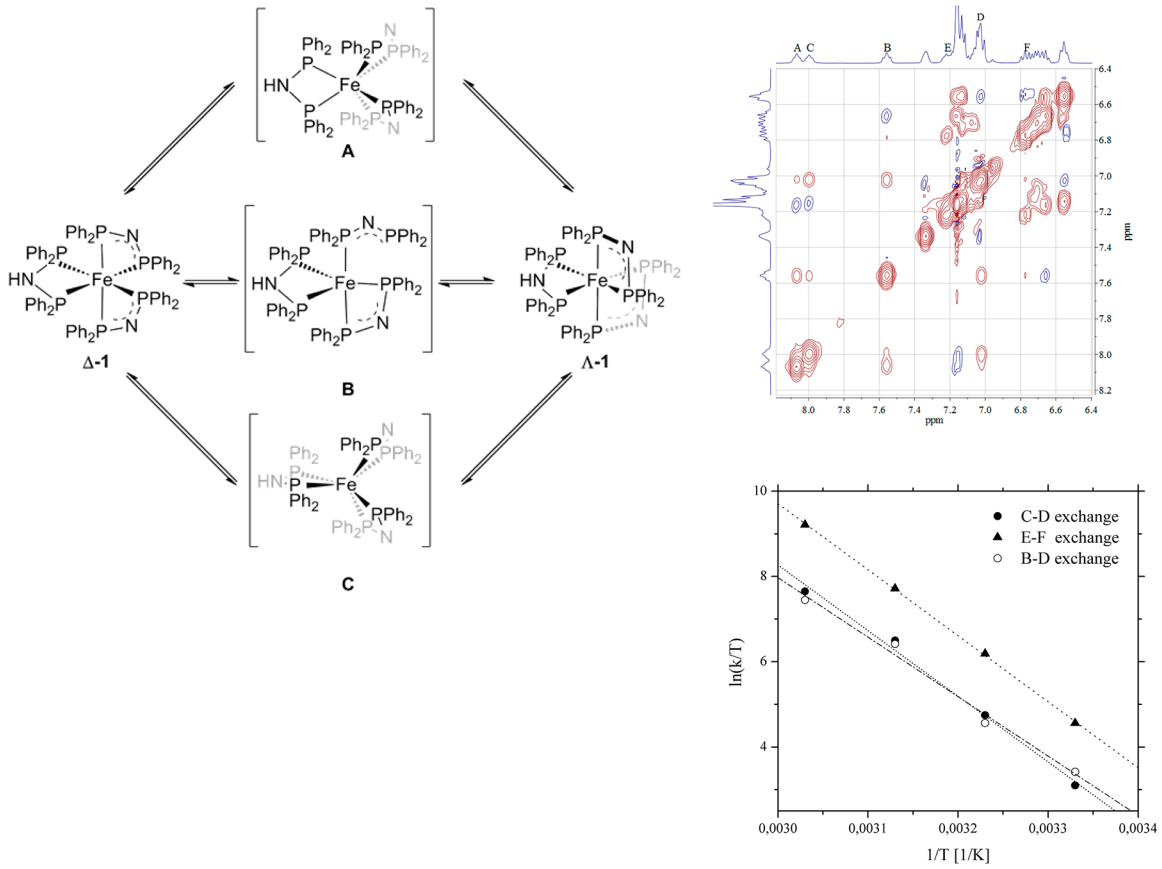

Figure 2. (left) Possible isomerization pathways of complex **1** in solution: Ray–Dutt twist (**A**); dissociative pathway (**B**); Bailar twist (**C**). (right, top) ^{1}H *g*NOESY NMR spectrum of complex **1**, showing cross-peaks due to NOE (blue) and chemical exchange (red). (right, bottom) Eyring analysis of the exchange rates in **1** obtained by variable-temperature ^{1}H *g*EXSY NMR measurements.

complexes.[18] Because of steric "overload", which is reflected in the rather long iron–phosphorus distances, a dissociative pathway for isomerization via a pentacoordinated transition state **B** also seems possible for complex **1**.

In order to gain further insights into the isomerization mechanism, we determined the rate constants for the chemical exchange of several *o*-phenyl resonances at different temperatures. Therefore, quantitative two-dimensional exchange spectroscopy (EXSY) NMR spectra were acquired following the procedure described in the review by Perrin and Dwyer.[19] It is worth mentioning that at low temperature there are two interfering dynamic processes. The lower exchange rate at low temperatures is expected to result in a line sharpening of the resonances in the ^{1}H NMR spectrum, but the hindered rotation of the phenyl groups in complex **1** subsequently causes an overall broadening at lower temperatures. For this reason, the rate constants were analyzed between 300 and 330 K.[20]

The Eyring analysis of the exchange of different *o*-phenyl protons is shown in Figure 2, and the corresponding enthalpies and entropies of activation are summarized in Table 1. For the four *o*-phenyl resonances of the two deprotonated dppa ligands (A–D), six exchange processes are theoretically possible, but only for three of them could reliable kinetic data be obtained. The two resonances corresponding to the protonated dppa ligand (E and F) are in exchange with each other, allowing analysis of the kinetic data.

The enthalpy of activation ($\Delta H^{\ddagger}$) for the exchange, which in part leads to an isomerization of the Δ and Λ isomers of **1**, was found to be between 116 and 140 kJ·mol^{-1}. A similar value of

Table 1. Activation Parameters for the Isomerization of Complex 1

resonances	$\Delta H^{\ddagger}$ [kJ·mol^{-1}]	$\Delta S^{\ddagger}$ [J·mol^{-1}·K^{-1}]
A and B	140 ± 4	204 ± 13
B and D	116 ± 9	211 ± 29
C and D	128 ± 8	255 ± 24
E and F	129 ± 2	269 ± 6

$\Delta H^{\ddagger}$ (118 ± 3 kJ·mol^{-1}) was found for the dicationic complex $[(phen)_3Fe]^{2+}$ (phen = 1,10-phenathroline), a complex known to undergo dissociative isomerization.[18] In accordance with the entropy of activation ($\Delta S^{\ddagger}$) of 89 ± 8 J·mol^{-1}·K^{-1} for $[(phen)_3Fe]^{2+}$, we determined a positive value of $\Delta S^{\ddagger}$ for complex **1**. However, the much larger $\Delta S^{\ddagger}$ value of 204–269 J·mol^{-1}·K^{-1} clearly points toward a dissociative isomerization process. At 11.6–18.9 kcal·mol^{-1} the corresponding Gibbs energies of activation at 298 K ($\Delta G^{\ddagger}_{298}$) are low enough for the reaction to proceed under mild conditions. Interestingly, the activation parameters for the exchange of the protonated and deprotonated ligand are similar. It should be emphasized at this point that not every exchange process results in isomerization and rather represents the exchange of protons between magnetically inequivalent phenyl groups. In addition, both the protonated and deprotonated dppa ligands exhibit dissociative exchange, resulting in different rate constants for the exchange processes.

Such a dissociative process could lead to the reversible generation of a vacant coordination site, making binding of

dx.doi.org/10.1021/ic5022164 | *Inorg. Chem.* 2014, 53, 11335–11343

Scheme 3. Reactivity of Complex 1 toward Dihydrogen

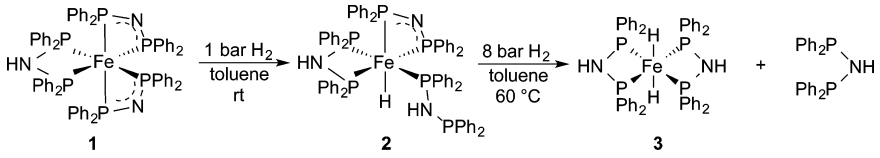

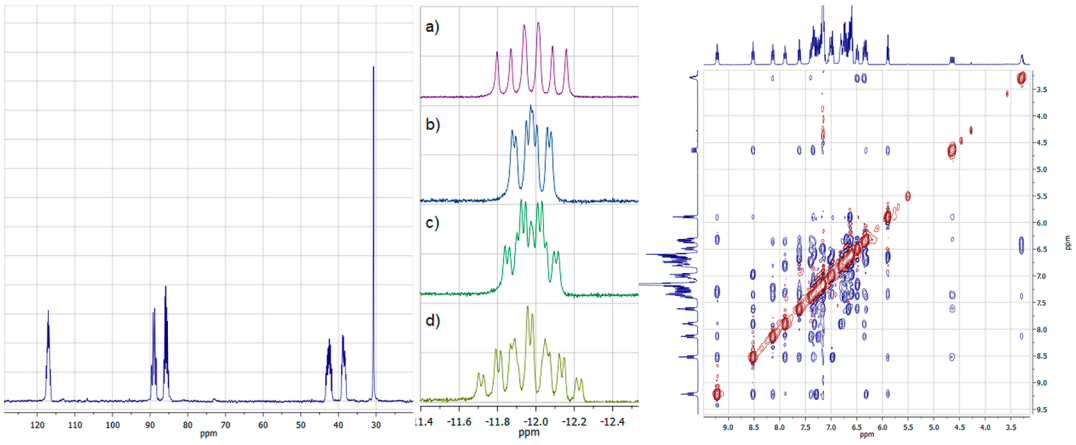

Figure 3. (left) $^{31}P\{^{1}H\}$ NMR spectrum of compound **2** in C_6D_6. (middle) Hydride resonance of complex **2** in the ^{1}H NMR spectrum (d), which simplifies upon ^{31}P decoupling with the decoupling frequency centered at (a) 40.0, (b) 87.0, or (c) 117.0 ppm. (right) ^{1}H *g*NOESY NMR spectrum of compound **2** in C_6D_6.

dihydrogen possible. As the two deprotonated dppa ligands can act as internal bases, heterolytic cleavage of dihydrogen should be facile. Accordingly, complex **1** was reacted with dihydrogen under various conditions. The reaction at ambient temperature and a hydrogen pressure of 1 bar resulted in slow conversion and the formation of a new complex **2** after a few days, while the reaction was significantly faster at higher hydrogen pressures (Scheme 3).

In comparison with **1**, which gives rise to three multiplet resonances in the $^{31}P\{^{1}H\}$ NMR spectrum, six resonances between 30 and 120 ppm can be observed after dihydrogen addition (Figure 3 left). Five of them are best described as multiplets, while the sixth resonance appears as a singlet at 30.7 ppm in the $^{31}P\{^{1}H\}$ NMR spectrum. As this signal is only slightly shifted in comparison to that of the free dppa ligand (43.1 ppm), it might correspond to an unbound arm of a κ^1-coordinated dppa ligand. In the ^{1}H NMR spectrum, a multiplet resonance between −11.6 and −12.2 ppm indicates the formation of an iron hydride complex. This resonance exhibits different multiplicities upon selective decoupling of the ^{31}P resonances (Figure 3 middle). In addition, a broad resonance at 3.29 ppm and a doublet of doublets resonance at 4.64 ppm ($^{2}J_{PH}$ = 18.0 Hz, 9.5 Hz) can be assigned to different NH protons of two inequivalent dppa ligands. The aromatic region of the ^{1}H NMR spectrum exhibits several signals, including five well-separated virtual triplet resonances that give rise to doublet resonances upon ^{31}P decoupling. The close proximity of all the aromatic protons is reflected in several NOE cross-peaks in the ^{1}H *g*NOESY NMR spectrum (Figure 3 right). Interestingly, no cross-peak due to chemical exchange with the same phase (color) as the diagonal peak can be observed in the spectrum, indicating the absence of exchange processes in complex **2**.

The molecular structure of complex **2** was confirmed using single-crystal X-ray diffraction (Figure 4). Complex **2** crystallizes in the triclinic space group $P\bar{1}$ with two formula units per unit cell. In comparison with **1**, the central iron(II)

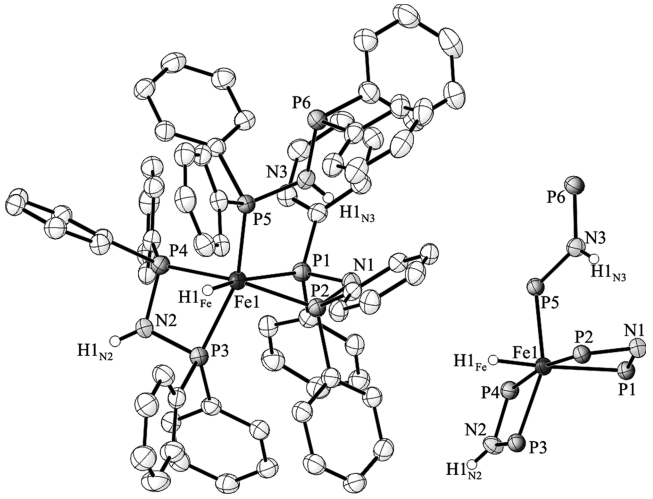

Figure 4. (left) ORTEP diagram of [(dppa)(Ph_2P–N–PPh_2)Fe(H)-(κ^1-Ph_2P–NH–PPh_2)$_2$] (**2**) with the thermal ellipsoids set at 50% probability (selected hydrogen atoms and solvent molecules have been omitted for clarity). (right) Connectivity of the heteroatoms in **2**. Selected distances [Å] and angles [deg]: Fe1–P1 2.279(1), Fe1–P2 2.295(1), Fe1–P3 2.240(1), Fe1–P4 2.234(1), Fe1–P5 2.219(1), Fe1–$H1_{Fe}$ 1.47(3); P4–Fe1–P3 71.73(4), P1–Fe1–P2 65.84(4), P5–Fe1–$H1_{Fe}$ 81.1(11).

atom in **2** is octahedrally coordinated by only five phosphine groups and one hydride ligand, originating from the heterolytic cleavage of dihydrogen. As the formed hydride ligand occupies one coordination site, the newly protonated dppa ligand binds to the iron(II) center through only one diphenylphosphino group, while the second group remains uncoordinated. While in the present case arm opening has been achieved by the reaction with H_2, in a previous study the formal insertion of BH_3 into the iron–phosphorus bond has been observed with deprotonated dppa as the ligand.[21]

dx.doi.org/10.1021/ic5022164 | *Inorg. Chem.* 2014, 53, 11335−11343

At 2.219(1) Å, the iron−phosphorus distance to the κ^1-coordinated dppa ligand is slightly shorter than the bond distances to the κ^2-coordinated dppa ligand [2.234(1)−2.240(1) Å] and the deprotonated κ^2-coordinated dppa ligand [2.279(1) − 2.295(1) Å]. Despite the fact that hydrides cannot be located accurately by single-crystal X-ray diffraction, a hydride ligand with an iron−hydrogen distance of 1.47(3) Å was found in the Fourier difference map and freely refined, in agreement with observations for previously reported iron(II) hydride complexes.[21,22] In the solid state, the dechelated ligand is oriented in such a way that the N3−$H1_{N3}$ bond points toward the deprotonated nitrogen atom N1 [N1···N3 = 3.407(3) Å], resulting in a rather long distance of 3.91(3) Å between $H1_{Fe}$ and $H1_{N3}$, which must have been formed after deprotonation of an intermediate dihydrogen complex. The absence of a proton bound to N1 is also evident from the corresponding P−Fe−P bite angle of 65.84(4)°, which is significantly smaller than the angle of the protonated ligand [71.73(4)°].

At ambient temperature, the initially formed complex **2** reacts very slowly and to a minor extent with a second equivalent of dihydrogen. Heating of complex **1** to 60 °C under a hydrogen pressure of 8 bar resulted in complete conversion of the starting complex and the formation of a red solid, **3**. This newly formed solid is extremely insoluble in common organic solvents. In C_6D_6, a quintet resonance of very weak intensity can be observed at −8.79 ppm in the ^{1}H NMR spectrum ($^2J_{PH}$ = 40.8 Hz), indicating that a strong donor ligand, such as a second hydride, is located at the *trans* position. In addition to the three resonances corresponding to phenyl hydrogen atoms between 7.00 and 7.60 ppm in the ^{1}H NMR spectrum, a broad signal at 3.27 ppm with the same integral as the hydride ligand can be detected. This resonance can be assigned to the N−H protons of the coordinated dppa ligands, which gives rise to the assumption that one protonated dppa ligand per hydride is present in **3**. The $^{31}P\{^1H\}$ NMR spectrum revealed a singlet resonance at 107.7 ppm, suggesting the formation of a symmetric complex such as a *trans*-dihydride. Additional evidence was provided by the IR spectrum of compound **3**, where a band of weak intensity was observed at 1714 cm^{-1}, while the Raman spectrum revealed a band at 1832 cm^{-1}; these bands can be assigned to the asymmetric and symmetric Fe−H vibrations, respectively, and point toward a centrosymmetric dihydride complex.

A careful structural analysis of single crystals formed during the reaction with dihydrogen in toluene/*n*-hexane confirmed the assumption that **3** is an octahedral *trans*-dihydride iron(II) complex (Figure 5). The central iron atom in **3** is coordinated by two coplanar dppa ligands and two hydride ligands at the apical positions, therewith adopting a *trans* arrangement. At 2.145(2)−2.150(2) Å (Table 2), the iron−phosphorus distances in **3** are rather short, while the hydride ligands, which could be located in the electron density map, were freely refined with Fe−H distances of 1.47(5)−1.57(6) Å.[22] The distortion from the idealized inversion symmetry is reflected in the angle formed by the two hydride ligands in the *trans* orientation and the central iron atom, which was found to be around 176(3)°.

In both reactions with H_2, the initial formation of a dihydrogen complex prior to the heterolytic cleavage is assumed. As bis(dialkylphosphino)amines are known to engage in tautomerization between the phosphinoamine and phosphanimine forms, deprotonation in the first step can generally

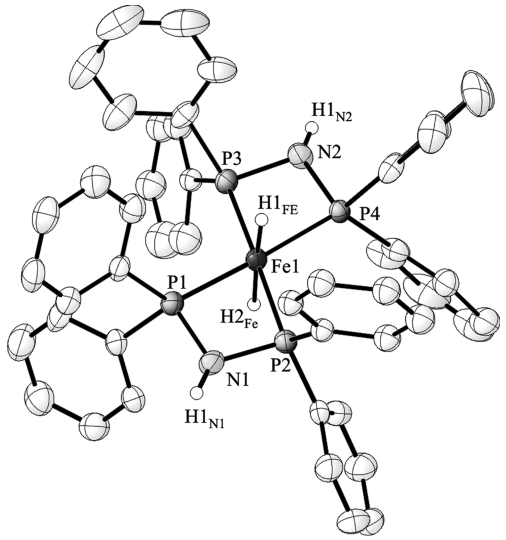

Figure 5. ORTEP diagram of *trans*-[(dppa)$_2$Fe(H)$_2$] (**3**) with the thermal ellipsoids set at 50% probability (selected hydrogen atoms and solvent molecules have been omitted for clarity). Selected distances [Å] and angles [deg]: Fe1−P1 2.150(2), Fe1−P2 2.150(2), Fe1−P3 2.145(2), Fe1−P4 2.146(1), Fe1−$H1_{Fe}$ 1.47(5), Fe1−$H2_{Fe}$ 1.57(6), N1−$H1_{N1}$ 0.89(7), N2−$H1_{N2}$ 0.75(5); P1−Fe1−P2 73.07(6), P3−Fe1−P4 72.71(5), P4−Fe1−P1 176.50(7), P3−Fe1−P2 176.35(7), $H1_{Fe}$−Fe1−$H2_{Fe}$ 176(3).

proceed via the phosphide group or the amide group of the opened arm.[23] In contrast, such an arm-opening event appears more unlikely in the formation of complex **3**.

To further examine the unusual properties of complexes **1** and **2**, we investigated their redox chemistry using cyclic voltammetry. As hydride ligands in iron(II) and ruthenium(II) complexes are known to become significantly more acidic upon oxidation to the corresponding iron(III) or ruthenium(III) species,[24] complexes that are able to cleave dihydrogen heterolytically can potentially serve as electrocatalysts for the formal conversion of dihydrogen into protons and electrons.[16c] Because of the ability of complex **1** to cleave dihydrogen to form complex **2**, in which the iron center is still bound to a deprotonated dppa ligand, a potential internal base, we were interested in whether the corresponding iron(III) hydride complex is acidic enough to get deprotonated. For this reason, we investigated the redox behavior of **1** and **2** in methylene chloride using cyclic voltammetry. Figure 6 shows the cyclic voltammograms (CVs) of complexes **1** and **2** in CH_2Cl_2 with different initial scan directions. The voltammogram of **1** with the initial positive scan direction (Figure 6a, blue solid line) exhibits an irreversible one-electron oxidation wave with an anodic peak potential of −0.21 V vs Fc/Fc^+ (Fc = ferrocene), which was assigned to the Fe^{II}/Fe^{III} couple of complex **1**. In addition, two irreversible oxidation waves with lower anodic peak currents at 0.48 and 0.85 V were observed using a scan rate of 100 mV/s. At lower scan rates, an additional irreversible wave was found at 0.03 V. A plot of the peak current versus the square root of the scan rate is linear only in the case of the first oxidation wave at −0.21 V, indicating that the redox processes corresponding to the waves at 0.03 and 0.48 V are not under diffusion control. Moreover, the current rather increases with decreasing scan rate for the wave at 0.03 V, indicating a chemical reaction after the initial oxidation followed by oxidation of the newly formed species (ECE mechanism).[25] By comparison with the CV of the free dppa ligand in CH_2Cl_2,

dx.doi.org/10.1021/ic5022164 | *Inorg. Chem.* 2014, 53, 11335−11343

Table 2. Comparison of Bond Lengths and Angles in Complexes 1−3

	1	2	3
Fe−P [Å]	2.316(1)−2.367(1)	2.219(1)−2.295(1)	2.145(2)−2.150(2)
N_{PPh_2} [a]	6	5	4
∠P*−Fe−P* [deg] [b]	65.56(4)−65.71(4)	65.84(4)	−
∠P−Fe−P [deg] [c]	69.24(4)	71.73(4)	72.71(5)−73.07(6)

[a]Number of coordinated PPh_2 groups. [b]P*−Fe−P* bite angle of the deprotonated dppa ligand. [c]P−Fe−P bite angle of the protonated dppa ligand.

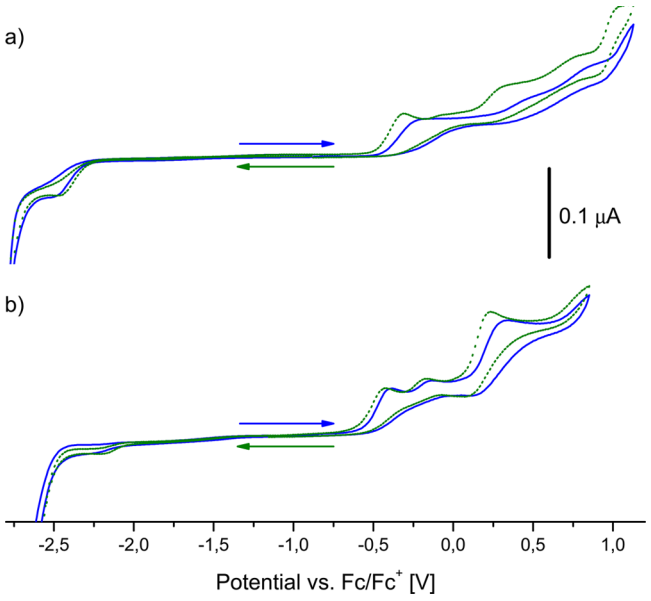

Figure 6. CVs of (a) complex **1** and (b) complex **2** in CH_2Cl_2 with different initial scan directions (1 mM, scan rate = 100 mV/s, Pt//0.1 M $^nBu_4NPF_6$//Pt).

the oxidation wave above 1.00 V in the CV of **1** was assigned to the irreversible oxidation of the uncoordinated phosphine ligand, while the redox wave at 0.85 is likely related to the oxidation of a coordinated dppa ligand. An irreversible one-electron reduction wave was observed at −2.50 V vs Fc/Fc^+, which was assignable to the Fe^I/Fe^{II} couple. Upon reversal of the initial scan direction (Figure 6a, green dotted line), the reduction wave remains unchanged, but the following oxidation waves exhibit higher peak currents and are slightly shifted to lower potentials, indicating passivation of the platinum electrode during the reduction.

The CV of complex **2** is shown in Figure 6b. An irreversible one-electron oxidation with a peak potential at −0.41 V was assigned to the Fe^{II}/Fe^{III} couple of complex **2**. A second irreversible redox process with a lower peak current is observed at −0.18 V. On the basis of the similarity of this peak potential to that of the Fe^{II}/Fe^{III} couple of complex **1**, we assume that the generated iron(III) hydride reacts to form a cationic iron(II) complex **D** and an iron(III) dihydrogen complex **E**, as previously observed for cyclopentadienyl-based iron complexes (Scheme 4).[16a] The third oxidation wave in the CV of **2** was attributed to the oxidation of a coordinated dppa/dppa* ligand.

Interestingly, the approximated half-height potentials ($E_{1/2}$) for the Fe^{II}/Fe^{III} couples of the two complexes do not obey the empirical rule of Lever,[26] which on average predicts half-height potentials of 1.456 V vs Fc/Fc^+ for the Fe^{II}/Fe^{III} couple of $[(L)_6Fe]^{2+}$ and 0.585 V vs Fc/Fc^+ for that of $[Fe(H)(L)_5]^+$, where L denotes every coordinated Ph_2P group of the coordinated bidentate bisphosphine.[20] The significantly higher $E_{1/2}$ values and the huge deviation of the predicted potential difference between the two complexes from the observed value reflect the lability of the dppa ligands in complex **1** and underline the previously discussed trend that with increasing number of coordinated Ph_2P groups the steric repulsion causes much weaker bonding. In line with these findings, the ligand parameters E_L derived from our experimental data are much smaller than the averaged E_L values reported by Lever for similar ligands (0.36−0.43),[20] whereas the value for **2** (0.19) is, as expected, higher than the value for **1** (0.12).

CONCLUSION

We have demonstrated that hemilability can occur in transition-metal complexes with homofunctional ligand systems and shown that the coordination number and the bite angle of a bidentate ligand can be varied to effect hemilability instead of combining different donor properties in one ligand. In the present case, the combination with an internal base allowed heterolytic cleavage of dihydrogen, thus combining the hemilabile nature of the dppa ligand with a cooperative site. The extension of this concept to catalytic applications as well as

Scheme 4. Proposed Reaction Pathway upon Oxidation of Complex 2

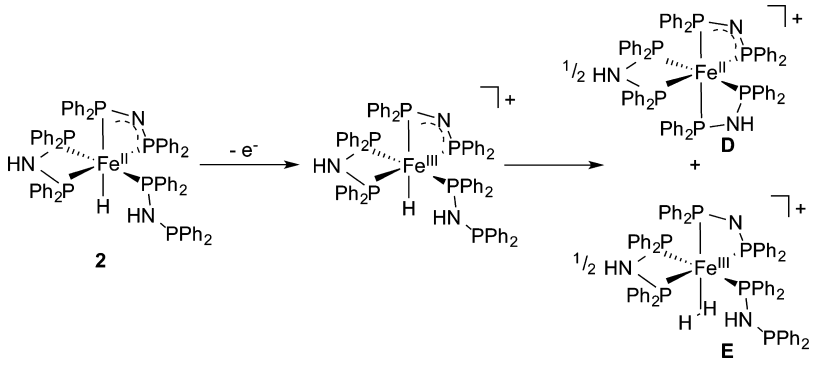

dx.doi.org/10.1021/ic5022164 | Inorg. Chem. 2014, 53, 11335−11343

Table 3. Crystallographic Data for 1−3

	1·C_7H_8	2·$^1/_2C_7H_8$	3
empirical formula	$C_{79}H_{69}FeN_3P_6$	$C_{72}H_{63}FeN_3P_6·^1/_2C_7H_8$	$C_{48}H_{44}FeN_2P_4$
formula weight [g·mol^{-1}]	1302.04	1257.99	828.58
T [K]	100(2)	100(2)	100(2)
crystal system	orthorhombic	triclinic	monoclinic
space group	$P2_12_12_1$	$P\bar{1}$	$P2_1/c$
a [Å]	13.137(3)	12.502(3)	18.359(1)
b [Å]	22.186(4)	14.942(3)	10.005(1)
c [Å]	24.594(5)	18.299(4)	22.171(1)
α [deg]	90	94.91(3)	90
β [deg]	90	101.53(3)	90.367(2)
γ [deg]	90	106.56(3)	90
V [Å^3]	7168(2)	3173.2(12)	4072.1(3)
Z	4	2	4
ρ_{calc} [g·cm^{-3}]	1.207	1.309	1.352
μ(Mo Kα) [mm^{-1}]	0.388	0.436	0.565
F(000)	2720	1306	1728
2θ range [deg]	1.986−53.52	1.976−53.50	4.98−53.46
measured reflections	54234	29010	57649
ind. reflections	15156	13336	8652
R_{int}	0.0898	0.0375	0.0855
ind. reflections [$I > 2\sigma(I)$]	11653	8763	6398
parameters/restraints	732/0	763/0	500/0
R1 [$I > 2\sigma(I)$]	0.0579	0.0402	0.0810
wR2 (all data)	0.1297	0.0956	0.1922
GOF (all data)	0.966	0.883	0.995
Flack parameter	0.016(18)	−	−
max. peak/hole [e·Å^{-3}]	0.820/−0.702	1.600/−0.342	0.487/−0.973
absorption correction	numerical	numerical	numerical
min/max transm.	0.9255/0.9666	0.8818/0.9530	0.932/1.000

to other transition metals is currently under investigation and discloses promising prospects.

EXPERIMENTAL SECTION

General. All of the experiments were carried out under an atmosphere of purified argon in a Braun Labmaster glovebox or using standard Schlenk techniques. Toluene and C_6D_6 were dried over Na/K alloy, and *n*-hexane was dried over $LiAlH_4$. The dppa ligand[27] and [Fe(N(SiMe$_3$)$_2$)$_2$(thf)][28] were prepared according to previously reported procedures. ^{1}H, ^{13}C, and ^{31}P NMR spectra were recorded using Bruker DRX 400, DRX 500, and Avance 500 NMR spectrometers. ^{1}H, ^{13}C{^{1}H}, and ^{13}C-APT (*a*ttached *p*roton *t*est) NMR chemical shifts are reported in parts per million downfield from tetramethylsilane. The resonance of the residual protons in the deuterated solvent was used as an internal standard for ^{1}H NMR spectra. The solvent peak of the deuterated solvent was used as an internal standard for ^{13}C NMR spectra. ^{31}P NMR chemical shifts are reported in parts per million downfield from H_3PO_4 and referenced to an external 85% solution of phosphoric acid in D_2O. The following abbreviations are used for the description of NMR data: br (broad), s (singlet), d (doublet), t (triplet), m (multiplet), v (virtual). IR spectra were recorded by attenuated total reflectance of the solid samples on a Bruker Tensor IF37 spectrometer. The intensities of the absorption bands are indicated as vw (very weak), w (weak), m (medium), s (strong), vs (very strong), and br (broad). High-resolution electrospray ionization (HR-ESI) and high-resolution atmospheric pressure chemical ionization (HR-APCI) mass spectra were acquired with an LTQ-FT mass spectrometer (Thermo Fischer Scientific). In both cases, the resolution was set to 100.000. Elemental analyses were performed on a Vario Micro Cube elemental analyzer.

Single-Crystal X-ray Analysis. The single-crystal X-ray diffraction data for the structural analyses were collected using graphite-monochromatized Mo Kα radiation [λ(Mo Kα) = 0.71073 Å] on a STOE IPDS2 (2·$^1/_2C_7H_8$) or IPDS2T (1·C_7H_8) imaging plate detector system or on a BRUKER D8 QUEST pixel detector system (3). The structures were solved by direct methods with SHELXS-97 and refined against F^2 by full-matrix least-squares techniques using SHELXL-97.[29] On the basis of the crystal descriptions, numerical absorption corrections were applied.[30] The crystallographic data for 1−3 have been deposited at the Cambridge Crystallographic Data Centre (CCDC 1009585−1009587) and can be obtained free of charge via www.ccdc.cam.ac.uk/. Details of the data collection and refinement are summarized in Table 3.

Synthesis of [(dppa)Fe(Ph$_2$P−N−PPh$_2$)$_2$] (1). [Fe(N(SiMe$_3$)$_2$)$_2$(thf)] (150 mg, 0.33 mmol) was dissolved in 12 mL of *n*-hexane to give a greenish solution, which was added slowly to a solution containing dppa (387 mg, 1.00 mmol) in 12 mL of toluene. The resulting dark-brown solution was allowed to stand at ambient temperature. Complex 1 started to crystallize after 90 min. After 6 days the solution was decanted off, and the crystals were dried in vacuo. Yield: 294 mg (0.24 mmol, 72%). Anal. Calcd for $C_{72}H_{61}Fe_1N_3P_6·C_7H_8$ (M = 1302.10 g/mol): C, 72.87%; H, 5.34%; N, 3.23%. Found: C, 73.13%; H, 5.84%; N, 3.20%. In the following NMR assignments, dppa* denotes a deprotonated ligand. ^{1}H NMR (400 MHz, C_6D_6, 27 °C) δ: 4.61 (s br, 1H, $\Delta\nu_{1/2}$ = 16.9 Hz, P−N*H*−P), 6.55 (t, 8H, $^3J_{HH}$ = 6.9 Hz, phenyl-H_{para} + toluene-*H*), 6.62−6.83 (m, 14H, phenyl-H_{meta} + dppa-H_{ortho}), 6.98−7.09 (m, 20H, toluene-*H* + phenyl-H_{meta} + dppa*-H_{ortho}), 7.10−7.15 (m superimposed, 8H, phenyl-H_{meta}), 7.22 (br superimposed, 4H, dppa-H_{ortho}), 7.30−7.37 (m, 4H, toluene-*H*), 7.56 (t, 4H, ^3J = 8.4 Hz, dppa*-H_{ortho}), 8.00 (t br, 4H, ^3J = 7.0 Hz, dppa*-H_{ortho}), 8.07 (t br, 4H, ^3J = 7.2 Hz, dppa*-H_{ortho}) ppm. ^{31}P{^{1}H} NMR (161 MHz, C_6D_6, 27 °C) δ: 4.0−5.2 (m, 2P, dppa*), 12.0−14.0 (m, 2P, dppa*), 64.0−65.7 (m, 2P, dppa) ppm. Selectively decoupled ^{1}H{^{31}P} NMR spectra were acquired, causing a changed multiplicity for some of the signals. In the following, only resonances that changed upon ^{31}P decoupling are reported. All of the other ^{1}H NMR

dx.doi.org/10.1021/ic5022164 | Inorg. Chem. 2014, 53, 11335−11343

resonances remained unchanged in comparison to the ^{1}H NMR spectrum reported above. ^{1}H{^{31}P} NMR (400 MHz, C_6D_6, 27 °C, with selective decoupling on the resonance centered at 64.8 ppm) δ: 4.61 (s br, 1H, $\Delta\nu_{1/2}$ = 10.0 Hz, P−N*H*-P) ppm. ^{1}H{^{31}P} NMR (400 MHz, C_6D_6, 27 °C, with selective decoupling on the resonance centered at 13.0 ppm) δ: 4.61 (t, 1H, $^2J_{PH}$ = 5.7 Hz, $\Delta\nu_{1/2}$ = 4.9 Hz, P−N*H*−P), 7.67 (d, 4H, $^3J_{HH}$ = 7.3 Hz, dppa*-H_{ortho}), 8.11 (d, 4H, $^3J_{HH}$ = 7.2 Hz, dppa*-H_{ortho}), 8.18 (d, 4H, $^3J_{HH}$ = 7.4 Hz, dppa*-H_{ortho}) ppm. ^{13}C-APT NMR (100.6 MHz, CD_2Cl_2, 27 °C) δ: 125.6 (s, toluene-*C*), 126.5 (s, phenyl-*C*), 126.8 (t, J_{PC} = 4.0 Hz, phenyl-*C*), 127.0 (t, J_{PC} = 4.8 Hz, phenyl-*C*), 127.3 (t, J_{PC} = 4.1 Hz, phenyl-*C*), 127.4 (s, phenyl-*C*), 129.3 (s, toluene-*C*), 129.7 (s, toluene-*C*), 130.4−130.7 (m br, phenyl-*C*), 130.8 (s, phenyl-*C*), 130.9 (s, phenyl-*C*), 131.1 (t, $^2J_{PC}$ = 4.2 Hz, phenyl-C_{ortho}), 131.5 (t, $^2J_{PC}$ = 4.4 Hz, phenyl-C_{ortho}), 132.5 (t, $^2J_{PC}$ = 4.4 Hz, phenyl-C_{ortho}), 137.8 (s, toluene-*C*), 139.4 (d, $^1J_{PC}$ = 28.5 Hz, phenyl-C_{ipso}), 145.0 (d, $^1J_{PC}$ = 32.1 Hz, phenyl-C_{ipso}), 145.8 (d, $^1J_{PC}$ = 24.1 Hz, phenyl-C_{ipso}), 147.0 (d, $^1J_{PC}$ = 26.3 Hz, phenyl-C_{ipso}), 151.7 (d, $^1J_{PC}$ = 11.5 Hz, phenyl-C_{ipso}), 152.5 (d, $^1J_{PC}$ = 26.4 Hz, phenyl-C_{ipso}) ppm. IR (ATR) $\tilde{\nu}$: 3051 (w), 2992 (vw), 2306 (w), 1548 (vw), 1478 (w), 1432 (m), 1304 (vw), 1261 (vw), 1206 (w), 1175 (w), 1087 (m), 1026 (w), 1002 (w), 970 (m), 853 (m), 752 (w), 731 (m), 722 (s), 525 (m), 494 (s), 465 (s), 441 (w) cm^{-1}. APCI-MS (pos., *m*/*z*): 386.1222 ([dppa + H]$^+$).

Synthesis of [(dppa)(Ph$_2$P−N−PPh$_2$)Fe(H)(κ^1-Ph$_2$P−NH−PPh$_2$)$_2$] (2). For the synthesis of complex **2**, the isolated or in situ-generated complex **1** could be used as the starting material. In a typical procedure, [Fe(N(SiMe$_3$)$_2$)$_2$(thf)] (113 mg, 0.25 mmol) was dissolved in 6 mL of toluene, and the resulting solution was added slowly to a solution of dppa (190 mg, 0.50 mmol, 2 equiv) in 6 mL of toluene. The resulting dark-yellow to brown solution was transferred to a 90 mL Fischer−Porter tube and charged with hydrogen to a pressure of 9 bar. After 2 days, complete conversion of complex **1** and formation of complex **2** was confirmed using ^{31}P{^{1}H} NMR spectroscopy. The reaction mixture was filtered, and the filtrate was layered with 40 mL of *n*-hexane, resulting in the formation of red crystals. Yield: 63 mg (0.05 mmol, 30% based on dppa). Anal. Calcd for $C_{72}H_{63}FeN_3P_6$ (*M* = 1211.98 g/mol): C, 71.35%; H, 5.24%; N, 3.47%. Found: C, 71.75%; H, 5.40%; N, 3.42%. ^{1}H NMR (400 MHz, C_6D_6, 27 °C) δ: −12.17 to −11.64 (m, 1H, Fe−*H*), 3.24−3.29 (br m, 1H, dppa N−*H*), 4.64 (dd, 1H, $^2J_{PH}$ = 18.0 Hz, $^2J_{PH}$ = 9.5 Hz, κ-Ph$_2$P−N*H*−PPh$_2$), 5.89 (t, 2H, $^3J_{HH}$ = 6.8 Hz, phenyl-*H*), 6.30−6.38 (m, 4H, phenyl-*H*), 6.49 (dd, 2H, $^3J_{HH}$ = 10.1 Hz, $^3J_{HH}$ = 7.4 Hz, phenyl-*H*), 6.58−6.81 (m, 18H, phenyl-*H*), 6.95−7.02 (m, 6H, phenyl-*H*), 7.14−7.41 (m, 18H, phenyl-*H*), 7.62 (vt, 2H, *J* = 8.3 Hz, phenyl-H_{ortho}), 7.90 (t, 2H, *J* = 8.3 Hz, phenyl-H_{ortho}), 8.13 (dd, 2H, $^3J_{PH}$ = 10.1 Hz, $^3J_{HH}$ = 7.5 Hz, phenyl-H_{ortho}), 8.52 (vt, 2H, *J* = 8.2 Hz, phenyl-H_{ortho}), 9.22 (t, 2H, *J* = 8.7 Hz, phenyl-H_{ortho}) ppm. ^{13}C-APT NMR (101 MHz, C_6D_6, 27 °C) δ: 126.2 (s, phenyl-*C*), 129.7 (s, phenyl-*C*), 129.9 (s, phenyl-*C*), 130.1 (s, phenyl-*C*), 130.5 (d, J_{PC} = 7.1 Hz, phenyl-*C*), 131.5 (s, phenyl-*C*), 131.8 (d, J_{PC} = 11.1 Hz, phenyl-*C*), 133.2 (s, phenyl-*C*), 133.4 (d, J_{PC} = 8.1 Hz, phenyl-*C*), 133.8 (s, phenyl-*C*), 134.8 (s, phenyl-*C*), 135.0 (s, phenyl-*C*), 136.9 (d, $^1J_{PC}$ = 71.7 Hz, phenyl-C_{ipso}), 141.2 (s, phenyl-C_{ipso}), 143.4 (d, $^1J_{PC}$ = 41.6 Hz, phenyl-C_{ipso}), 145.1 (d, $^1J_{PC}$ = 41.0 Hz, phenyl-C_{ipso}), 150.5 (d, $^1J_{PC}$ = 33.6 Hz, phenyl-C_{ipso}) ppm. ^{31}P{^{1}H} NMR (161 MHz, C_6D_6, 27 °C) δ: 31.67 (s, 1P, Fe−Ph$_2$P−N*H*−PPh$_2$), 38.4−39.5 (m, 1P), 41.1−42.7 (m, 1P), 85.4−86.6 (m, 1P), 87.8−89.1 (m, 1P), 116.9−118.1 (m, 1P) ppm. IR (ATR) $\tilde{\nu}$: 3446 (w), 3053 (w), 2002 (vw), 1584 (vw), 1569 (vw), 1476 (w), 1432 (m), 1303 (w), 1272 (w), 1248 (w), 1196 (w) 1177 (w), 1154 (w), 1088 (m), 1025 (w), 999 (w), 910 (m), 852 (m), 830 (m), 817 (m), 743 (m), 732 (m), 688 (vs), 616 (s), 551 (s), 524 (s), 442 (w), 420 (w), 406 (w) cm^{-1}. APCI-MS (pos., *m*/*z*): 386.1222 (100%, [dppa + H]$^+$), 880.0871 (20%, [(dppa*)$_2$Fe$_2$]$^+$), 1265.1944 (30%, [(dppa*)$_3$Fe$_2$ + H]$^+$).

Synthesis of *trans*-[(dppa)$_2$Fe(H)$_2$] (3). For the synthesis of complex **3**, the isolated complex **1** or **2** or the in situ-generated complex **1** could be used as the starting material. In a typical procedure, [Fe(N(SiMe$_3$)$_2$)$_2$(thf)] (113 mg, 0.25 mmol) was dissolved in 6 mL of toluene, and the resulting solution was added slowly to a solution of dppa (190 mg, 0.50 mmol, 2 equiv) in 6 mL of toluene. The resulting dark-yellow to brown solution was transferred to a 90 mL Fischer−Porter tube, charged with hydrogen to a pressure of 9 bar, and heated to 60 °C. After 21 h red crystals formed, which were separated and dried under vacuum. Yield: 62 mg (0.075 mmol, 30% based on [Fe(N(SiMe$_3$)$_2$)$_2$(thf)]). Anal. Calcd for $C_{48}H_{44}FeN_2P_4$ (*M* = 828.62 g/mol): C, 69.58%; H, 5.35%; N, 3.38%. Found: C, 69.25%; H, 5.50%; N, 3.68%. Complex **3** was extremely insoluble in all organic solvents that were available to us. As the measurement of meaningful ^{1}H and ^{31}P{^{1}H} NMR spectra already required prolonged acquisition times, ^{13}C NMR analysis was not possible for this complex. ^{1}H NMR (400 MHz, C_6D_6, 27 °C) δ: −8.79 (quint, 2H, $^2J_{PH}$ = 40.8 Hz, Fe−*H*), 3.27 (s, 2H, N−*H*), 6.90−7.57 (m, 40H, phenyl-*H*) ppm. ^{31}P{^{1}H} NMR (161 MHz, C_6D_6, 27 °C) δ: 107.7 (s) ppm. In the following, only the resonance whose multiplicity changed upon ^{31}P decoupling is reported: ^{1}H{^{31}P} NMR (400 MHz, C_6D_6, 27 °C) δ: −8.79 (s, 2H, Fe−*H*) ppm. IR (ATR) $\tilde{\nu}$: 3727 (vw), 3704 (vw), 3627 (vw), 3596 (vw), 3325 (w), 3066 (vw), 3050 (vw), 2360 (vs), 2341 (m), 1714 (w, $\nu_{Fe-H_{asym}}$), 1584 (vw), 1570 (vw), 1546 (vw), 1478 (w), 1432 (m), 1388 (vw), 1306 (vw), 1261 (vw), 1165 (m), 1097 (m), 769 (m), 739 (m), 690 (m), 669 (m), 535 (m), 515 (m), 493 (m) cm^{-1}. Raman (crystalline sample) $\tilde{\nu}$: 1832 (vw, $\nu_{Fe-H_{sym}}$), 1586 (w), 1482 (vw), 1438 (vw), 1183 (vw), 1160 (vw), 1101 (m), 1072 (vw), 1031 (w), 1002 (s), 927 (vw), 912 (vw), 868 (vw), 788 (vw), 747 (vw), 707 (w), 693 (vw), 621 (vw), 562 (vs), 508 (vw), 487 (vw), 466 (w), 402 (vw), 360 (w), 271 (vw), 257 (vw), 229 (vw), 216 (vw), 202 (w), 166 (m), 114 (s), 80 (s) cm^{-1}. APCI-MS (pos., *m*/*z*): 386.1222 (100%, [dppa + H]$^+$), 441.0492 (20%, [(dppa)Fe]$^+$), 825.1563 (25%, [(dppa)$_2$Fe − H]$^+$), 826.1625 (25%, [(dppa)$_2$Fe(H)$_2$]$^+$).

■ ASSOCIATED CONTENT

Ⓢ Supporting Information

NMR spectra of the complexes, variable-temperature NMR measurements, and further information on the cyclic voltammetry measurements. This material is available free of charge via the Internet at http://pubs.acs.org.

■ AUTHOR INFORMATION

Corresponding Author

*Fax: (+)49-6421-2825653. E-mail: robert.langer@chemie.uni-marburg.de.

Notes

The authors declare no competing financial interest.

■ ACKNOWLEDGMENTS

R.L. is grateful to Prof. S. Dehnen and Prof. C. v. Hänisch for their continuous support and assistance. This research was supported by the Deutsche Forschungsgemeinschaft (DFG) and the Erich-Becker-Foundation.

■ REFERENCES

(1) (a) Grützmacher, H. *Angew. Chem.* **2008**, *120*, 1838−1842; *Angew. Chem., Int. Ed.* **2008**, *47*, 1814−1818. (b) Schneider, S.; Meiners, J.; Askevold, B. *Eur. J. Inorg. Chem.* **2012**, 412−429. (c) van der Vlugt, J. I. *Eur. J. Inorg. Chem.* **2012**, 363−375. (d) Noyori, R.; Koizumi, M.; Ishii, D.; Ohkuma, T. *Pure Appl. Chem.* **2001**, *73*, 227−232. (e) Ikariya, T.; Blacker, A. J. *Acc. Chem. Res.* **2007**, *40*, 1300−1308. (f) Johnson, N. B.; Lennon, I. C.; Moran, P. H.; Ramsden, J. A. *Acc. Chem. Res.* **2007**, *40*, 1291−1299.

(2) (a) Milstein, D. *Top. Catal.* **2010**, *53*, 915−923. (b) Gunanathan, C.; Milstein, D. *Science* **2013**, *341*, 249−261.

(3) (a) Zuo, W.; Lough, A. J.; Li, Y. F.; Morris, R. H. *Science* **2013**, *342*, 1080−1083. (b) Morris, R. H. *Chem. Soc. Rev.* **2009**, *38*, 2282−2291. (c) Gaillard, S.; Renaud, J. *ChemSusChem* **2008**, *1*, 505−509. (d) Sui-Seng, C.; Freutel, F.; Lough, A. J.; Morris, R. H. *Angew. Chem.* **2008**, *120*, 954−957; *Angew. Chem., Int. Ed.* **2008**, *47*, 940−943. (e) Mikhailine, A.; Lough, A. J.; Morris, R. H. *J. Am. Chem. Soc.* **2009**,

131, 1394−1395. (f) Enthaler, S.; Hagemann, B.; Erre, G.; Junge, K.; Beller, M. *Chem.—Asian J.* **2006**, *1*, 598−604. (g) Zhou, S.; Fleischer, S.; Junge, K.; Das, S.; Addis, D.; Beller, M. *Angew. Chem.* **2010**, *122*, 8298−8302; *Angew. Chem., Int. Ed.* **2010**, *49*, 8121−8125. (h) Yang, J.; Tilley, T. D. *Angew. Chem.* **2010**, *122*, 10384−10386; *Angew. Chem., Int. Ed.* **2010**, *49*, 10186−10188.

(4) (a) Bart, S. C.; Lobkovsky, E.; Chirik, P. J. *J. Am. Chem. Soc.* **2004**, *126*, 13794−13807. (b) Bart, S. C.; Hawrelak, E. J.; Lobkovsky, E.; Chirik, P. J. *Organometallics* **2005**, *24*, 5518−5527. (c) Trovitch, R. J.; Lobkovsky, E.; Bill, E.; Chirik, P. J. *Organometallics* **2008**, *27*, 1470−1478.

(5) (a) Casey, C. P.; Guan, H. *J. Am. Chem. Soc.* **2007**, *129*, 5816−5817. (b) Casey, C. P.; Guan, H. *J. Am. Chem. Soc.* **2009**, *131*, 2499−2507.

(6) (a) Langer, R.; Leitus, G.; Ben-David, Y.; Milstein, D. *Angew. Chem., Int. Ed.* **2011**, *50*, 2120−2124. (b) Langer, R.; Diskin-Posner, Y.; Leitus, G.; Shimon, L. J. W.; Ben-David, Y.; Milstein, D. *Angew. Chem., Int. Ed.* **2011**, *50*, 9948−9952. (c) Langer, R.; Iron, M. A.; Konstantinovski, L.; Diskin-Posner, Y.; Leitus, G.; Ben-David, Y.; Milstein, D. *Chem.—Eur. J.* **2012**, *18*, 7196−7209.

(7) (a) Slone, C. S.; Weinberger, D. A.; Mirkin, C. A. *Prog. Inorg. Chem.* **1999**, *48*, 233−350. (b) Braunstein, P.; Naud, F. *Angew. Chem., Int. Ed.* **2001**, *40*, 680−699. (c) Basetti, M. *Eur. J. Inorg. Chem.* **2006**, 4473−4482.

(8) (a) Gunanathan, C.; Gnanaprakasam, B.; Iron, M. A.; Shimon, L. J. W.; Milstein, D. *J. Am. Chem. Soc.* **2010**, *132*, 14763−14765. (b) Klerman, Y.; Ben-Ari, E.; Diskin-Posner, Y.; Leitus, G.; Shimon, L. J. W.; Ben-David, Y.; Milstein, D. *Dalton Trans.* **2008**, 3226−3234. (c) Vuzman, D.; Poverenov, E.; Shimon, L. J. W.; Diskin-Posner, Y.; Milstein, D. *Organometallics* **2008**, *27*, 2627−2634. (d) Poverenov, E.; Gandelman, M.; Shimon, L. J. W.; Rozenberg, H.; Ben-David, Y.; Milstein, D. *Organometallics* **2005**, *24*, 1082−1090. (e) Poverenov, E.; Leitus, G.; Shimon, L. J. W.; Milstein, D. *Organometallics* **2005**, *24*, 5937−5944.

(9) (a) Gunanathan, C.; Ben-David, Y.; Milstein, D. *Science* **2007**, *317*, 790−792. (b) Balaraman, E.; Gnanaprakasam, B.; Shimon, L. J. W.; Milstein, D. *J. Am. Chem. Soc.* **2010**, *132*, 16756−16758. (c) Gnanaprakasam, B.; Milstein, D. *J. Am. Chem. Soc.* **2011**, *133*, 1682−1685.

(10) Kiss, G.; Horváth, I. *Organometallics* **1991**, *10*, 3798−3799.

(11) (a) Enthaler, S.; Junge, K.; Beller, M. *Angew. Chem.* **2008**, *120*, 3363−3367; *Angew. Chem., Int. Ed.* **2008**, *47*, 3317−3321. (b) Bolm, C.; Legros, J.; Le Paih, J.; Zani, L. *Chem. Rev.* **2004**, *104*, 6217−6254. (c) Correa, A.; Mancheño, O. G.; Bolm, C. *Chem. Soc. Rev.* **2008**, *37*, 1108−1117.

(12) Clapham, S. E.; Hadzovic, A.; Morris, R. H. *Coord. Chem. Rev.* **2004**, *248*, 2201−2237.

(13) Lagaditis, P. O.; Sues, P. E.; Sonnenberg, J. F.; Wan, K. Y.; Lough, A. J.; Morris, R. H. *J. Am. Chem. Soc.* **2014**, *136*, 1367−1380.

(14) (a) Suess, D. L. M.; Peters, J. C. *J. Am. Chem. Soc.* **2013**, *135*, 4938−4941. (b) Brown, S. D.; Mehn, M. P.; Peters, J. C. *J. Am. Chem. Soc.* **2005**, *127*, 13146−13147. (c) Brown, S. D.; Peters, J. C. *J. Am. Chem. Soc.* **2004**, *126*, 4538−4539. (d) Bart, S. C.; Lobkovsky, E.; Bill, E.; Chirik, P. J. *J. Am. Chem. Soc.* **2006**, *128*, 5302−5303.

(15) Fong, H.; Moret, M.-E.; Lee, Y.; Peters, J. C. *Organometallics* **2013**, *32*, 3053−3062.

(16) (a) Liu, T.; Chen, S.; O'Hagan, M. J.; DuBois, M. R.; Bullock, R. M.; DuBois, D. L. *J. Am. Chem. Soc.* **2012**, *134*, 6257−6272. (b) Henry, R. M.; Shoemaker, R. K.; DuBois, D. L.; DuBois, M. R. *J. Am. Chem. Soc.* **2006**, *128*, 3002−3010. (c) Liu, T.; DuBois, D. L.; Bullock, R. M. *Nat. Chem.* **2013**, *5*, 228−233. (d) Liu, T.; Wang, X.; Hoffmann, C.; DuBois, D. L.; Bullock, R. M. *Angew. Chem.* **2014**, *126*, 5404−5408.

(17) (a) Gilbertson, J. D.; Szymczak, N. K.; Crossland, J. L.; Miller, W. K.; Lyon, D. K.; Foxman, B. M.; Davis, J.; Tyler, D. R. *Inorg. Chem.* **2007**, *46*, 1205−1214. (b) Kashiwabara, K.; Ozeki, Y.; Kita, M.; Fujita, J.; Nakajima, K. *Bull. Chem. Soc. Jpn.* **1995**, *68*, 3453−3457.

(18) Jordan, R. B. *Reaction Mechanisms of Inorganic and Organometallic Systems*; Oxford University Press: New York, 1991; pp 91−118.

(19) Perrin, C. L.; Dwyer, T. J. *Chem. Rev.* **1990**, *90*, 935−967.

(20) For a detailed description, please see the Supporting Information.

(21) Frank, N.; Hanau, K.; Flosdorf, K.; Langer, R. *Dalton Trans.* **2013**, *42*, 11252−11261.

(22) (a) Gao, Y.; Holah, D. G.; Hughes, A. N.; Spivak, G. J.; Havighurst, M. D.; Magnuson, V. R.; Polyakov, V. *Polyhedron* **1997**, *16*, 2797−2807. (b) Gao, Y.; Holah, D. G.; Hughes, A. N.; Spivak, G. J.; Havighurst, M. D.; Magnuson, V. R. *Polyhedron* **1998**, *17*, 3881−3888. (c) Ellermann, J.; Gabold, P.; Schelle, C.; Knoch, F. A.; Moll, M.; Bauer, W. *Z. Anorg. Allg. Chem.* **1995**, *621*, 1832−1843.

(23) Barry, B. M.; Dickie, D. A.; Murphy, L. J.; Clyburne, J. A. C.; Kemp, R. A. *Inorg. Chem.* **2013**, *52*, 8312−8314.

(24) (a) Chen, J.; Szalda, D. J.; Fujita, E.; Creutz, C. *Inorg. Chem.* **2010**, *49*, 9380−9391. (b) Smith, K.-T.; Ramming, C.; Tilset, M. *J. Am. Chem. Soc.* **1993**, *115*, 8681−8689.

(25) Heinze, J. *Angew. Chem.* **1984**, *96*, 823−840; *Angew. Chem., Int. Ed. Engl.* **1984**, *23*, 831−847.

(26) (a) Lever, A. B. P. *Inorg. Chem.* **1990**, *29*, 1271−1285. (b) Lever, A. B. P. *Inorg. Chem.* **1991**, *30*, 1980−1985.

(27) Nöth, H.; Meinel, L. *Z. Anorg. Allg. Chem.* **1967**, *349*, 225−240.

(28) Olmstead, M. M.; Power, P. P.; Shoner, S. C. *Inorg. Chem.* **1991**, *30*, 2547−2551.

(29) Sheldrick, G. M. *Acta Crystallogr., Sect. A* **2008**, *64*, 112−122.

(30) (a) *X-SHAPE: Crystal Optimisation for Numerical Absorption Correction Program*, version 1.06; Stoe & Cie GmbH: Darmstadt, Germany, 1999. (b) *X-RED32: Data Reduction Program*, version 1.01; Stoe & Cie GmbH: Darmstadt, Germany, 2001.